

Aerodynamic loading of a typical low-rise building for an experimental stationary and non-Gaussian impinging jet

Chowdhury Jubayer*, Djordje Romanic^a and Horia Hangan^b

Wind Engineering, Energy and Environment (WindEEE) Research Institute, Western University, London, Ontario, Canada

(Received September 7, 2018, Revised February 26, 2019, Accepted February 28, 2019)

Abstract. Non-synoptic winds have distinctive statistical properties compared to synoptic winds and can produce different wind loads on buildings and structures. The current study uses the new capabilities of the WindEEE Dome at Western University to replicate a stationary non-Gaussian wind event recorded at the Port of La Spezia in Italy. These stationary non-Gaussian wind events are also known as intermediate wind events as they differ from non-stationary non-Gaussian events (e.g., downbursts) as well as stationary Gaussian events (e.g., atmospheric boundary layer (ABL) flows). In the present study, the wind loads on a typical low-rise building are investigated for an intermediate wind event reproduced using a continuous radial impinging jet (IJ) at the WindEEE Dome. For the same building model, differences in wind loads between ABL and IJ are also examined. Wind loads on different surface zones on the building, as defined in the ASCE code for design loads, are also calculated and compared with the code.

Keywords: non-Gaussian; impinging jet; low-rise building; wind load; WindEEE Dome

1. Introduction

Separation of thunderstorm from non-thunderstorm wind events is typically based on inspection of stationarity, Gaussianity, peak values, and gust factors from wind speed time series (Kasperski 2002, Cook *et al.* 2003, Lombardo *et al.* 2009, De Gaetano *et al.* 2014). For example, downbursts are strongly non-stationary and non-Gaussian wind events (Holmes and Oliver 2000, Holmes *et al.* 2008, Solari *et al.* 2015), whereas the standard synoptic winds are stationary and Gaussian (Gomes and Vickery 1977, Cook *et al.* 2003). Interestingly, De Gaetano *et al.* (2014) introduced a new class of wind events characterized by stationary, but non-Gaussian statistics. In addition, maximum wind speeds and gust factors associated with these intermediate events are larger compared to standard synoptic winds, but not as large as for the downburst events. Following the work of Kasperski (2002), De Gaetano *et al.* (2014) called these events gust fronts.

The statistical parameters used to differentiate between various types of wind events are derived from 10-minute samples of raw data. These statistics are mean wind speed (\bar{V}_{10}), the peak velocity averaged over 1 s (\hat{V}_1), gust factor ($G_{10} = \hat{V}_1/\bar{V}_{10}$), turbulence intensity (I_{10}), skewness (γ_{10}) and kurtosis (k_{10}). In some cases (De Gaetano *et al.* 2014), the same parameters are obtained for the time period of 1 hour instead of 10 minutes in order to assess the influence

of averaging window on the statistical properties of time series. For the stationary non-Gaussian wind event reported in De Gaetano *et al.* (2014) (cf. Fig. 4(a) in their paper) measured at 10 m above ground on 16 December 2011 in La Spezia, Italy, \bar{V}_{10} is relatively low (8.12 m s^{-1}), while \hat{V}_1 and I_{10} are comparably large (18.66 m s^{-1} and 0.38, respectively); hence $G_{10} = 2.30$. A departure from Gaussian distribution is indicated by $\gamma_{10} = 0.42$ (0) and $k_{10} = 2.60$ (3), with Gaussian values of parameters being in the brackets.

There is an increasing number of experimental and numerical studies on non-stationary and non-Gaussian wind events, such as downbursts (Letchford and Chay 2002, Chen and Letchford 2004a, Sengupta and Sarkar 2008, Xu and Hangan 2008, McConville *et al.* 2009, Hangan *et al.* 2019) and tornadoes (Mishra *et al.* 2008, Haan *et al.* 2010, Refan *et al.* 2014), and a vast literature on stationary and Gaussian atmospheric boundary layer (ABL) flows (Cermak 1971, Uematsu and Isyumov 1999, Holmes 2015, Jubayer and Hangan 2016). It seems, however, that there is a lack of experimental research addressing the stationary, non-Gaussian wind events. The absence of experimental studies on these intermediate winds is mainly due to the operational limitations of the traditional ABL wind tunnels, as well as of some non-synoptic wind simulators. These facilities are designed to physically simulate stationary Gaussian ABL flows or highly transient non-Gaussian downbursts or tornadoes (Letchford *et al.* 2002), respectively. Accordingly, significant advancements have been achieved in the estimation of design wind loads on structures due to the ABL winds, and to a lesser extent due to the downburst and tornadic flows. Wind tunnel tests with ABL flows are a basis for the loading codes around the world (e.g., AS / NZS 1170.2:2011 2015, NBCC 2010 2012, ASCE 7-10 2013). Previous studies on wind structure

*Corresponding author, Research Scientist, Ph.D.

E-mail: cjubaye@uwo.ca

^a Ph.D.,

E-mail: dromanica@uwo.ca

^b Professor,

E-mail: hmhangan@uwo.ca

interaction (Choi and Hidayat 2002, Chen and Letchford 2004b, Chay *et al.* 2006, Kwon and Kareem 2009, 2013, Solari *et al.* 2015) demonstrated that different statistical properties of wind events play a crucial role in the evaluation of wind-excited responses of structures. For these reasons, the impact of stationary and non-Gaussian wind events on buildings and structures deserves further investigation.

Chay and Letchford (2002) studied the pressure distribution on a cube at the geometric scale of 1:3000 using a stationary IJ. Their results show that the pressure distribution is similar to that obtained in wind tunnel tests with uniform flow. However, due to the higher turbulence in the IJ, variation of pressure distribution was observed in the separated flow regime when compared with conventional wind tunnel tests. The percentage difference of external pressure coefficients of approximately up-to 160% was observed on the roof and leeward wall. In a numerical study, Kim *et al.* (2007) performed computational fluid dynamics (CFD) simulations to evaluate wind loads on a tall building immersed in IJ flow. As the velocity varied with the radial position from the storm centre, the structural load on the building also varied, which was in correlation with the radial variation of the velocity profiles. As a result, base shear forces and base moments were higher in the IJ case compared to those in ABL, especially for larger jet diameters (> 2000 m). Radial positioning of the building with respect to the downburst centre is of significant importance as the maximum velocity, which in turn results in maximum shear force and base moment, is observed at a particular radial distance from the downburst centre (most cases at radial distance same as the jet diameter).

The main objective of this study is to provide experimental aerodynamic loading data for stationary but non-Gaussian wind events. As demonstrated above, these wind records represent an important part of the real wind events in mixed climates (De Gaetano *et al.* 2014). A new-generation wind facility—the Wind Engineering, Energy and Environment (WindEEE) Dome—at Western University in Canada has a unique capability of replicating stationary and Gaussian, as well as non-stationary and non-Gaussian flows (Hangan 2010, Hangan *et al.* 2017a, b, Junayed *et al.* 2019). Present study demonstrates an additional capability of this facility to simulate stationary non-Gaussian winds as a special case of a stationary impinging jet (IJ) flow. The persistent lack of the information on the physical nature and meteorological properties of these events does not authorize to say that they are produced in nature by a downdraft analogous to the one that occurs in thunderstorm downbursts. Under this point of view, the present study identifies a tool (IJ) to reproduce the wind speed of intermediate events by statistically matching with full scale intermediate event reported in De Gaetano *et al.* (2014), without any proof that such a tool reproduces also the physical phenomenon that creates these events.

In this study, wind loads on a typical low-rise building are investigated under a large laboratory simulated, stationary non-Gaussian IJ flow produced in the WindEEE Dome. The orientation of the building with respect to the IJ is varied and the pressure distribution on the surfaces of the

building is analyzed. Additional tests have been carried out on the same building model immersed in ABL flow in order to compare pressure distributions between stationary non-Gaussian (IJ) and stationary Gaussian (ABL) flows.

2. Experimental set-up

2.1 Stationary, non-Gaussian IJ simulation

The test chamber at the WindEEE Dome has a 25 m hexagonal footprint and a total of 100 fans installed on the periphery walls. Out of these 100 fans, 60 fans are mounted on one wall of the test chamber and another rest of the fans are distributed along the perimeter on the other five walls. The 6 other larger fans are in a plenum above the test chamber. This upper plenum is connected to the test chamber by a circular opening with bell-mouth and mechanical louvers. The height of the chamber (H), which is also the vertical distance between the jet outlet and the jet impinging surface, is 3.8 m. In this study, the 6 fans in the upper plenum were run with the mechanical louvers completely open to create the continuous radial IJ. A schematic of the flow at the WindEEE Dome is shown in Fig. 1 (Hangan 2014). The diameter of the circular opening (D) was set at 3.2 m providing an $H/D > 1$ ratio, which allows for fully development of the ring vortex above the surface (Xu and Hangan 2008) and is consistent with observations of full scale downburst events (Sengupta 2007; Zhang *et al.* 2013). For this study, WindEEE Dome was operated in the closed circuit mode with flow recirculating through the perimeter fans (Fig. 1).

2.2 ABL flow simulation

The WindEEE Dome can also be operated in a conventional ABL wind tunnel mode to produce synoptic straight winds. In the wind tunnel mode, the 60 fans on one wall of the test chamber are employed. A 1:3 two-dimensional contraction in plan, spires, trips and roughness blocks were used to generate the required ABL flow for this study. A schematic for the wind tunnel mode at the WindEEE Dome is shown in Fig. 2.

2.3 Building model

One of the generic low-rise buildings from the National Institute of Standards and Technology (NIST) database (Ho *et al.* 2005) at 1:100 geometric scale was used for the experiment. The model had the full-scale plan dimension of 57.15 m \times 36.57 m with eave height (h) of 12.19 m and roof slope of 1:12, see Fig. 3 for the scaled model. The model was instrumented with a total of 504 taps distributed on the surfaces of the building as shown with red dots in Fig. 4. The same building model was used for both the IJ and ABL flow configurations. The setups of the model in the test chamber for both flow configurations are shown in Fig. 5.

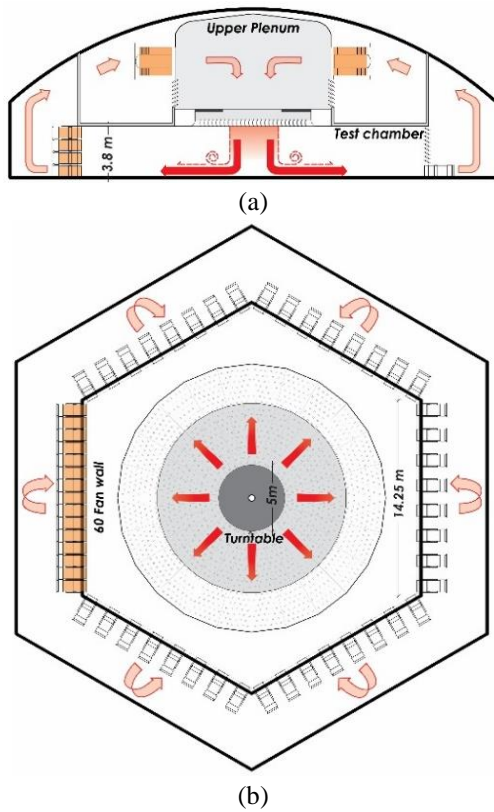


Fig. 1 Schematic of the IJ simulation at WindEEE Dome, (a) vertical section and (b) horizontal section

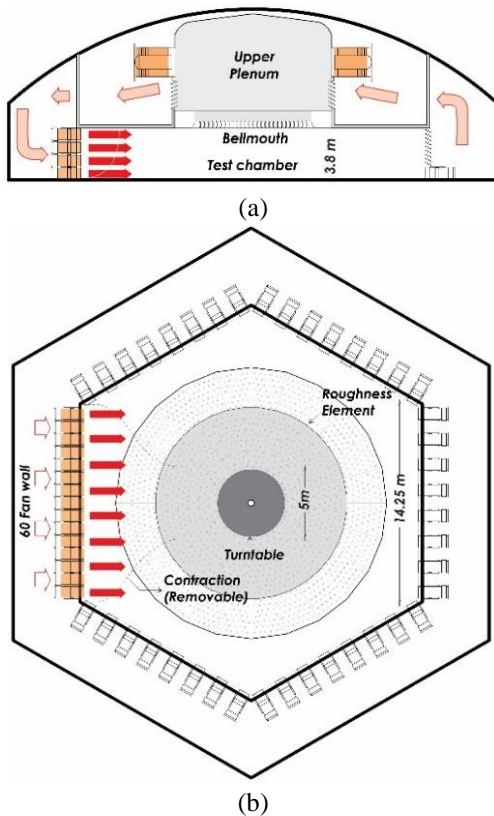


Fig. 2 Schematic of the ABL simulation at WindEEE Dome, (a) vertical section and (b) horizontal section

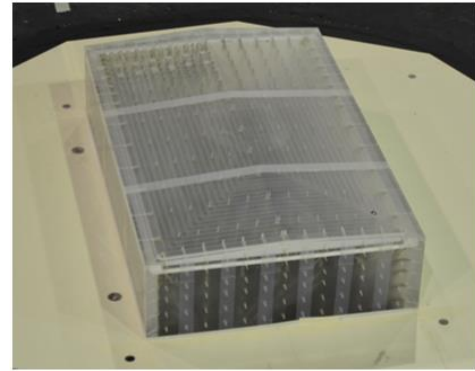


Fig. 3 Model of the building tested in this study

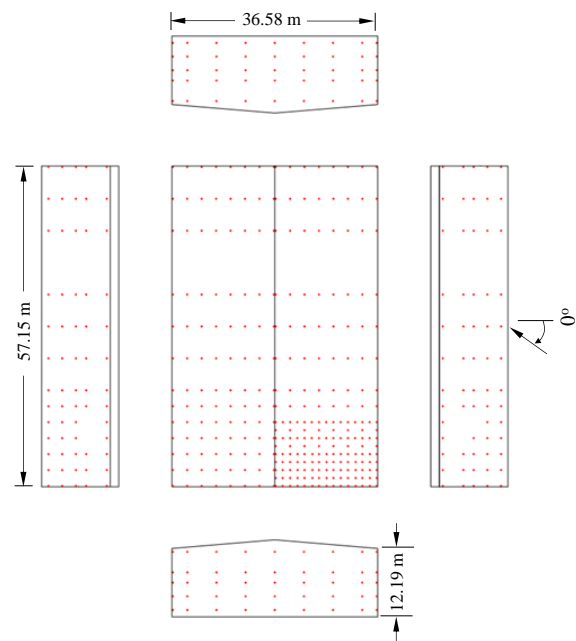
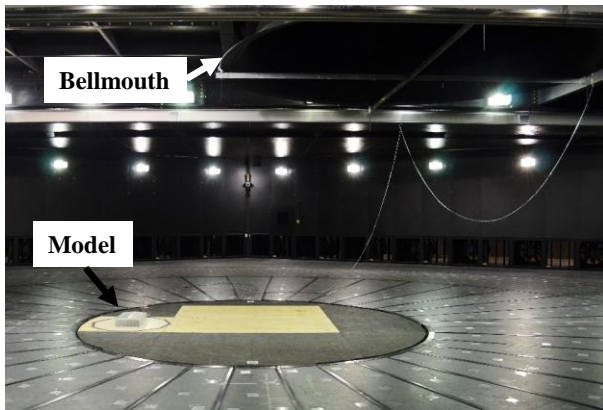


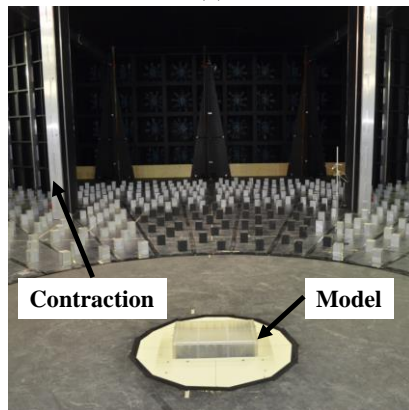
Fig. 4 Pressure tap distributions (dimensions are in full scale) on the tested building shown in Fig. 3

2.4 Pressure measurement system

A combination of rigid and flexible tubing system was used for surface pressure measurements in this study. In this setup, rigid brass tubes were at the tap and flexible Polyvinyl chloride (PVC) tubes were connected with the brass tube. Two 0.5 m long PVC tubes with 0.9 mm outer diameter were connected with a stainless steel restrictor. The restrictor tube was used to minimize the distortion effect caused by the tubing system on the pressure fluctuations (Surry and Stathopoulos 1978, Irwin *et al.* 1979). The tubing system was connected to the Electronically Scanned Pressure (ESP) scanners manufactured by the Pressure Systems, Inc. Pressure range of the scanners is ± 1 kPa. The proper and periodic calibration maintains the errors of the scanners within $\pm 0.03\%$. Digital Temperature Compensation (DTC) Initiium, also developed by the Pressure Systems, Inc., were used as the data acquisition system. The accuracy of the Initiium is \pm



(a)



(b)

Fig. 5 Building model in the test chamber for (a) IJ and (b) ABL flow

0.05% over the entire operating temperature range (0°C to 70°C). A Windows® based utility software written in Visual Basic was used to sample data, configure data acquisition parameters (e.g., sample rate, averaging) as well as diagnose errors (e.g., leak checks, channel status).

2.5 Test procedure

During the test for IJ, all 6 fans in the upper plenum were set at 20% of their rated RPM (1200). A total of three different cases, based on the building orientation, was studied. For all cases, the roughness elements in the test chamber were kept flush with the floor. Schematics of the three cases are shown in Fig. 6. The leading edge of the building was at $R/D = 0.9$ (R is the radial distance from the jet centre and D is the diameter of the jet equal to 3.2 m). Between Cases 1 and 2, the building was rotated by 90°. In Case 3, the building was oriented so that the radial velocity component acts towards the high density tap corner on the roof of the building at 57° with the short edge of the building footprint. With the building's full scale plan dimension of 57.15 m (length) by 36.58 m (width), the cornering angle is about 57° [$\tan^{-1}(57.15/36.58) = 57.4^\circ$] with the short edge of the building footprint. Cornering angle tends to produce peak wind loads on the roof of low-rise building in ABL flow (Ho *et al.* 2005). Although the current study employed an IJ, cornering angle is chosen for one of

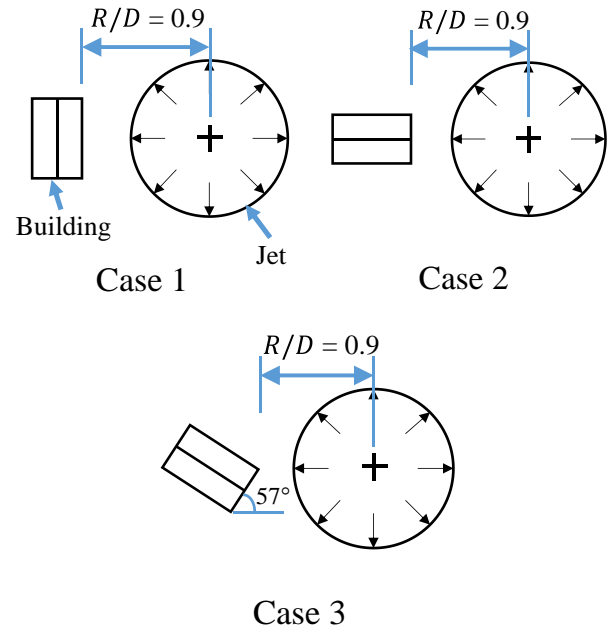


Fig. 6 Schematic of the test cases for IJ

the cases herein as well. For the ABL flow configuration, pressure measurements were taken at every 5° angular orientation of the building from 0° to 180°, including the corner angle (57°). However, results from the three matching angle cases (0°, 90° and 57°) from ABL are compared with IJ flow results. For both flow configurations, surface pressures were recorded at a sampling frequency of 500 Hz for 120 s.

3. Flow characteristics and statistics

3.1 Stationary IJ characterization

Cobra probes (four hole pressure probe) from Turbulent Flow Instrumentation Pty Ltd. were employed to determine the wind velocities in the empty chamber at different radial locations (R) from the jet centre ($R/D = 0.7, 0.8, 0.9, 1.0, 1.1, 1.2$) and at different heights (Z) from the floor ($Z/D = 0.003, 0.009, 0.016, 0.031, 0.047, 0.063, 0.079, 0.095, 0.138$). The velocity measurements were recorded at a sampling frequency of 1250 Hz for a sampling time of 120 s. The mean velocity profiles are presented in Fig. 7. The maximum mean radial velocity ($V_{Rmax} = 9.36 \text{ m s}^{-1}$) was measured at $R/D = 1.0$ and $Z/D = 0.016$. For all radial locations from the jet centre, the highest wind speed was found at the same height, $Z/D = 0.016$. Although the maximum mean radial velocity was found at $R/D = 1.0$, the locations from $R/D = 0.8$ to 1.0 at $Z/D = 0.016$ gave velocities very similar to V_{Rmax} with differences in wind speed of about 0.1 m s^{-1} . Heights shown in Fig. 7 are normalized with the height of the maximum mean radial velocity ($Z_{max} = 0.05 \text{ m}$) in the chamber. The turbulence intensity profiles are shown in Fig. 8. The turbulence intensity at the building height was approximately 9%.

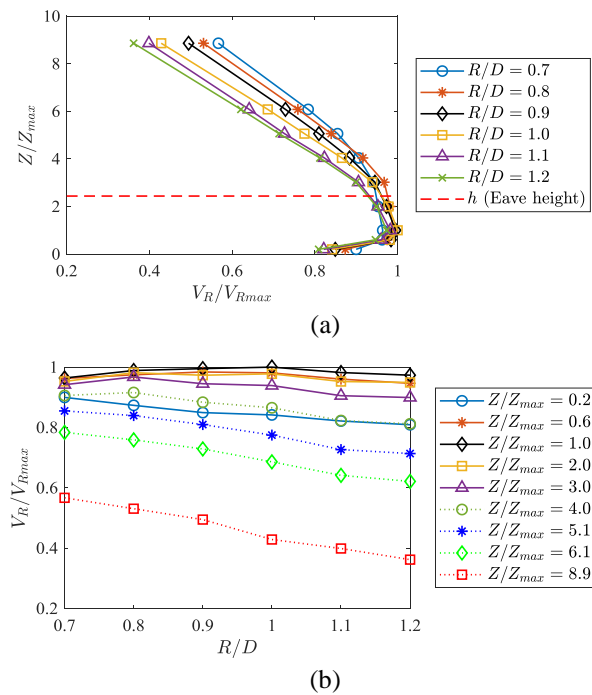


Fig. 7 Mean radial velocity profiles in the IJ plotted (a) vertically and (b) radially

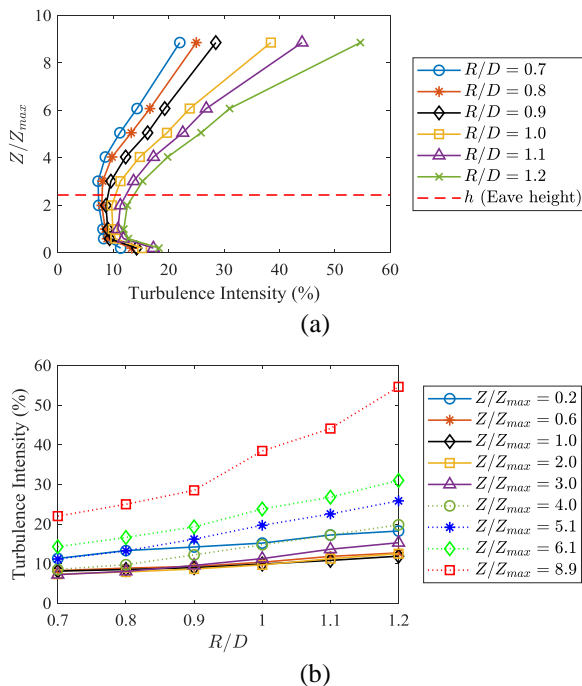


Fig. 8 Turbulence intensity profiles in the IJ plotted (a) vertically and (b) radially

Non-dimensional velocity profiles from the present study are compared with previous IJ studies by Chay and Letchford (2002) and Kim *et al.* (2007) (Fig. 9). A brief summary of these studies has been presented in Section 1. Profiles at three radial distances ($R/D = 1.00, 1.10, 1.20$)

from the present study are chosen to compare with profiles at $R/D = 1.00$ and 1.25 from Chay and Letchford (2002) and $R/D = 1.10$ from Kim *et al.* (2007). Six different jet diameters ($D = 500$ to 3000 m) were employed by Kim *et al.* (2007), out of which three ($D = 1000, 2000$ and 3000 m) are presented herein. As can be seen from Fig. 9, gradient in the velocity profiles from Chay and Letchford (2002) is lower compared to the present study and Kim *et al.* (2007). In general, the profiles from the present study match closer with Kim *et al.* (2007) compared to Chay and Letchford (2002). It is to be noted here that the sole intent of Fig. 9 is to compare, not to validate, the profiles from the present study using stationary non-Gaussian impinging jet with the profiles found in the literature using impinging jets.

The results of the present IJ are also compared to the stationary and non-Gaussian wind event reported by De Gaetano *et al.* (2014) (Fig. 10). This intermediate wind event was recorded on 05 December 2011 around 5:00 PM local time in the port of La Spezia, Italy, as part of a monitoring network created for the European projects “Wind and Ports” (Solari *et al.* 2012) and “Wind, Ports and Sea” (Repetto *et al.* 2017). The sampling frequency of the bi-axial ultrasonic anemometer that captured this event is 10 Hz and the instrument is positioned at 10 m above ground. The non-Gaussian properties of this event are evident after inspecting the skewness ($\gamma_{10} = 0.83$) and kurtosis ($k_{10} = 3.39$) of the central 10-minute segment of the time series as indicated in Fig. 10. In addition, the peak speed is $\hat{V}_1 = 15.90$ m s⁻¹, the gust factor is $G_{10} = 1.98$ and turbulence intensity is $I_{10} = 0.27$.

The wind record produced in the WindEEE Dome is shown in Fig. 11(a), while Fig. 11(b) shows the central 10 minutes of 1 hour data from Fig. 10.

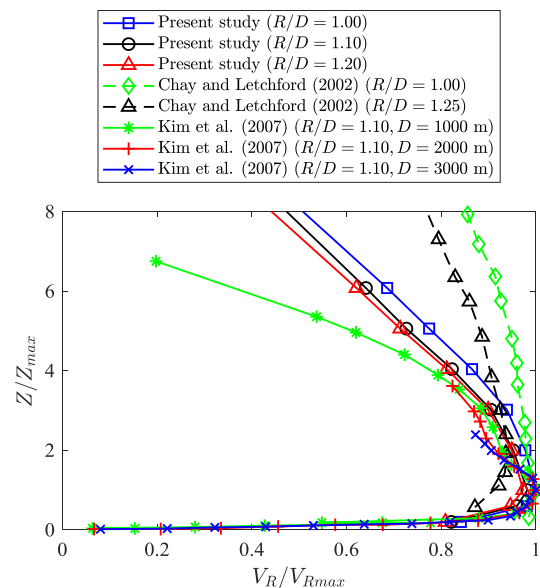


Fig. 9 Comparison of non-dimensional velocity profiles to previous IJ studies

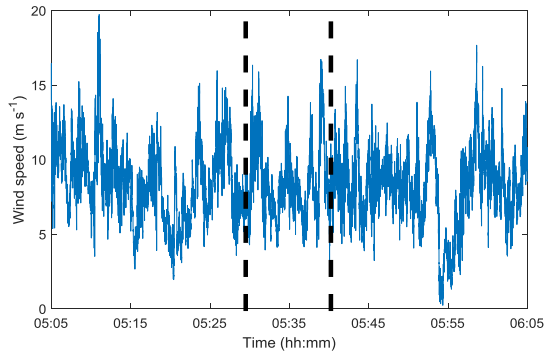


Fig. 10 1 hour of full scale wind speed data characterized with stationary but non-Gaussian statistics of the central 10-minute segment (dashed lines). The record was provided by De Gaetano *et al.* (2014)

The velocity scale between WindEEE Dome data and the full-scale event is determined as the ratio of 1 s peak velocities: $\hat{V}_{1FS}/\hat{V}_{1WD} = 15.90/13.42 = 1.20$, where the subscripts FS and WD denote the Full Scale and WindEEE Dome records, respectively. The time scale is determined by best matching the statistical properties ($\gamma_{10}, k_{10}, \hat{V}_1, I_{10}$) of the experimental and full scale data through a minimization function and the corresponding time scale of WindEEE Dome data is found to be 1:84. That is, a moving average filter of window length w is applied on the WindEEE Dome instantaneous data. Different values of w provide different values of comparative statistics between the WindEEE Dome and full scale data. The w value that provides the best similarity in terms of the statistical properties of WindEEE Dome data and full scale data is used to calculate time scale. Those statistical properties of WindEEE Dome data and full scale data are presented in Table 1. The largest discrepancy between these two time series is observed for I_{10} , where $I_{10FS} = 2.7I_{10WD}$. The corresponding length scale determined as the product of the time and velocity scales is 1:101, which closely matches the geometric scale of the tested building (1:100). It is important to note here that the similarity between the two time series is analyzed comparing the statistical properties of these two, and not the direct cross-correlation between the time series. That is, although the time series might look different in the time domain (Fig. 11), their statistical non-Gaussian properties are comparable with about 24% difference in skewness and 13% difference in kurtosis (Table 1). As discussed in Introduction, these statistical properties of wind events determine its loading characteristics (Choi and Hidayat 2002, Chen and Letchford 2004b, Chay *et al.* 2006; Kwon and Kareem 2009, 2013, Solari *et al.* 2015). Namely, γ_{10} and k_{10} are noticeably non-Gaussian in both cases, while the records are stationary without showing transient features such as the one observed, for example, for the downburst events.

Although the temporal characteristics are matched with intermediate wind events, the spatial characteristics (e.g., velocity profile with heights) of these events are still unknown. Since an IJ is employed here to reproduce the time dependent characteristics of the intermediate wind

events, the typical nose shape velocity profile for IJ is obtained. As wind loading depends on both temporal and spatial characteristics of the wind flow field, differences in velocity profile may influence the wind loads on buildings or other ground mounted structures. Further research, in particular more wind speed records from real events, is needed to fully define the shape of the vertical velocity profile for intermediate wind events. Fig. 11c shows that the spectra of experimental data and full scale data are similar. Small deviation from the reference $-5/3$ line is observed in the high-frequency domain of WindEEE Dome data.

3.2 ABL

The ABL flow generated for this study was at 1:100 geometric scale and for open terrain exposure. The flow was measured at the turn table centre in the absence of the building model using cobra probes. Wind speeds were sampled at 1250 Hz for 120 s. Normalized mean streamwise velocity (U) and turbulence intensity profiles obtained at the WindEEE Dome, along with the comparison with ESDU standards (ESDU 1982, 1983) for open terrain exposure (aerodynamic roughness length, $z_0 = 0.03$ m), are shown in Fig. 12(a). Mean streamwise velocities (U) are normalized with velocity at 50 m (U_{50m}).

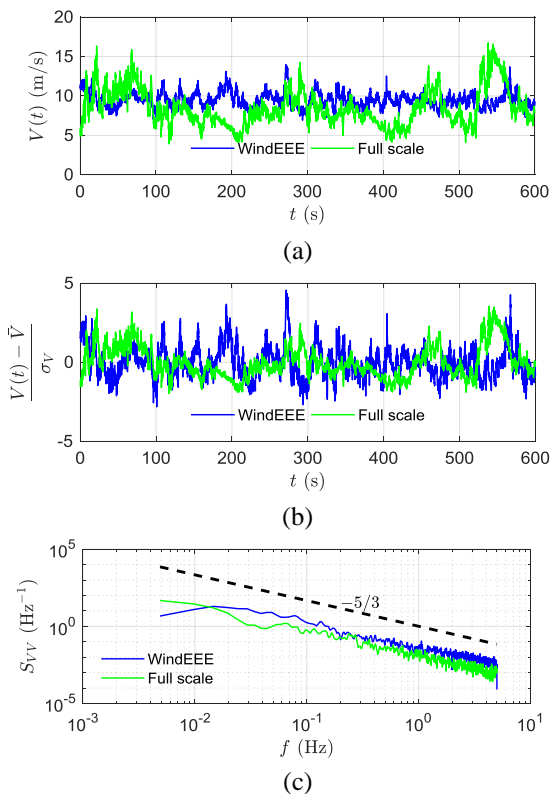


Fig. 11 (a) WindEEE Dome data that statistically match the full scale stationary and non-Gaussian wind event, (b) same as (a) but two time series are normalized, (c) wind spectra. Note that the full scale time series in (a) is the central 10 minutes of 1 hour data presented in Fig. 10

Table 1 Main synthetic statistical parameters of full scale and WindEEE Dome data

Time series	γ_{10}	k_{10}	\bar{V}_1 (m s ⁻¹)	I_{10}
Full scale	0.83	3.39	15.90	0.27
WindEEE Dome	0.65	3.86	13.42	0.10

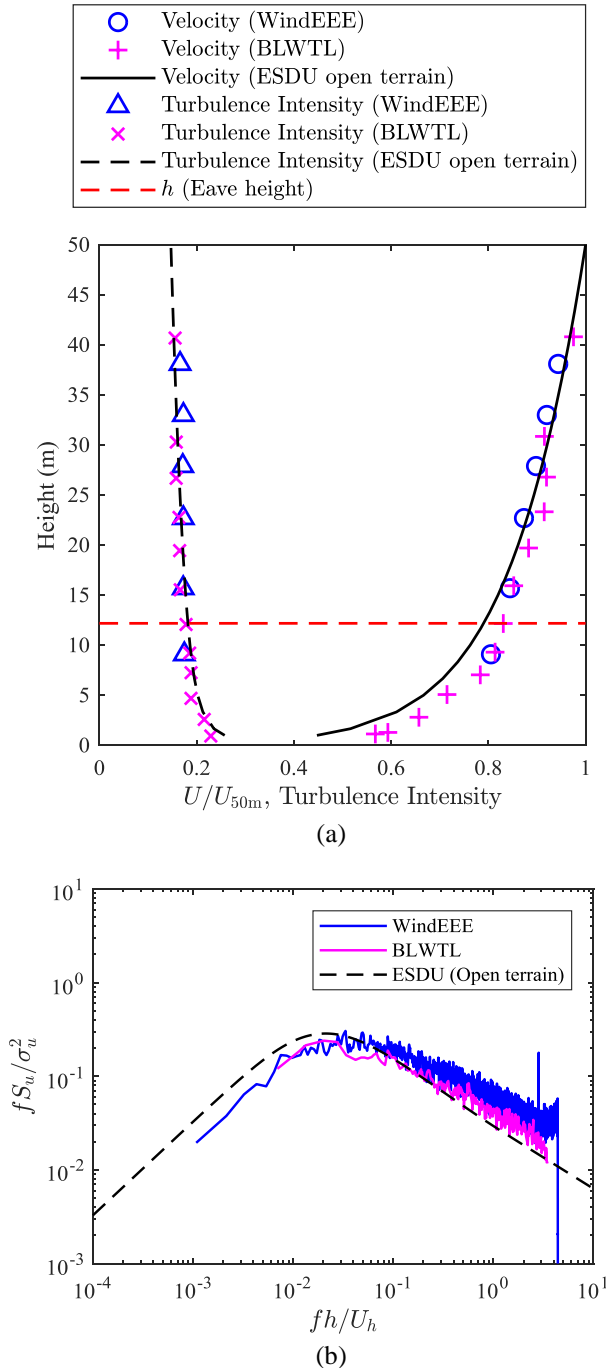


Fig. 12 (a) Velocity and turbulence intensity profiles and (b) wind spectra for the ABL flow at the WindEEE Dome and BLWTL with ESDU standard

Wind spectra at the building height from the WindEEE Dome along with ESDU standard (ESDU 1985) is provided in Fig. 12(b), where f is the frequency, S_u is the spectra of streamwise velocity fluctuation (u), σ_u is the standard deviation of the streamwise velocity fluctuation, h is the building eave height and U_h is the mean streamwise velocity at h . Velocity and turbulence intensity profiles as well as wind spectra from Boundary Layer Wind Tunnel Laboratory (BLWTL) for the NIST Database (Ho *et al.* 2005) are also shown in Fig. 12.

4. Results

4.1 Surface pressures

Pressure distributions on the building surfaces are presented in terms of pressure coefficients (C_p). C_p is calculated as

$$C_p = \frac{P - P_{ref}}{\frac{1}{2} \rho V_{ref}^2} \quad (1)$$

where, P is the pressure on the building surface, P_{ref} is the reference static pressure, ρ is the density of air (1.2 kg m⁻³) and V_{ref} is the reference mean velocity magnitude. In this study, the atmospheric pressure was used as the reference pressure for the IJ flow, whereas the static pressure at the gradient wind height was chosen as the reference pressure for ABL. For IJ, the maximum radial velocity was taken as the reference velocity ($V_{ref} = V_{Rmax} = 9.36$ m s⁻¹), while for ABL, the velocity at the building height was the reference velocity ($V_{ref} = U_h = 13.18$ m s⁻¹). The choice of reference static and dynamic pressures for non-synoptic wind events are still not standardized and have been under investigation by several researchers. Currently atmospheric pressure as reference static pressure is widely used to calculate pressure coefficients for non-synoptic wind events (Chay and Letchford 2002, Haan *et al.* 2010, Jubayer *et al.* 2016). On the other hand, using atmospheric pressure as reference pressure for ABL flow does not provide meaningful C_p . As can be seen from Fig. 13, using atmospheric pressure as the reference static pressure has produced reasonable C_p values (~ 1) around the stagnation region on the building surfaces for IJ (Fig. 13(a)). However for ABL flow, mean $C_p > 1$ around the stagnation region (Fig. 13(b)) indicates that using the atmospheric pressure as the reference static pressure would not provide a meaningful C_p comparison between IJ and ABL flows. The reference velocities for both IJ and ABL were recorded in the absence of the building. First, convergence of the mean C_p is checked for the

pressure tap that gave the maximum standard deviation of pressure for each of the IJ cases (Fig. 14). The mean C_p 's have converged at about 40 s for all three cases, which confirms that the sampling time of 120 s is sufficient for the analysis of the data.

4.1.1 Mean pressure coefficients

Mean C_p contours for the three IJ cases along with the three ABL cases are shown in Fig. 15. As pointed out previously, the orientation of the building in Cases 1, 2 and 3 for IJ flow resemble with 0° , 90° and 57° wind direction cases for ABL respectively. Overall, the mean C_p distributions on the building surfaces for the IJ case seem qualitatively similar to those in ABL flows (Fig. 15). The mean C_p is maximum on the windward wall for both ABL and IJ. Except the windward wall, all other surfaces of the building experience negative pressures. For the corner angle case, conical shape pressure distributions on the roof indicate the possible presence of corner vortices. A closer look indicates that the mean roof suction is higher in ABL compared to that in IJ flow. In order to provide a quantitative comparison, mean C_p profiles are plotted along a line on the building surfaces for all building orientations.

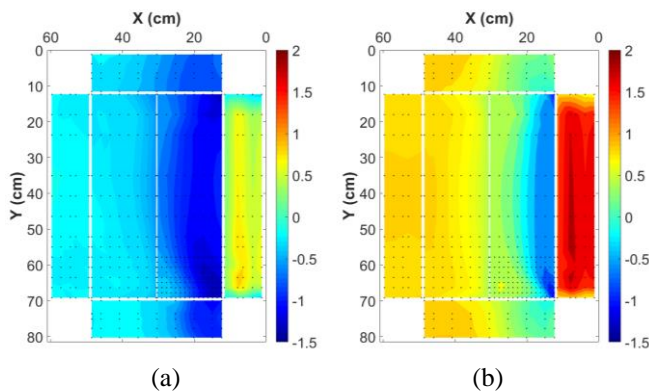


Fig. 13 Mean C_p contours using atmospheric pressure as the reference static pressure for (a) IJ Case 1 and (b) ABL 0°

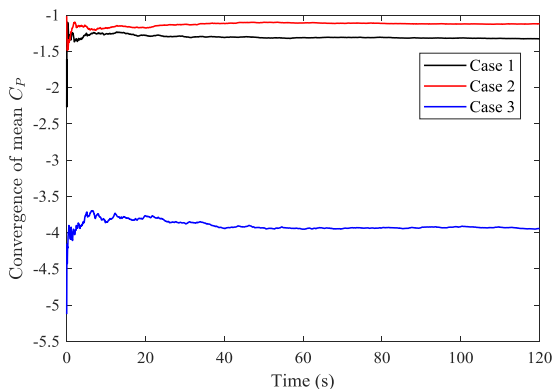


Fig. 14 Convergence of mean C_p in the IJ flow

The line of taps along which the profiles are plotted are shown in Fig. 16. For Case 2, the taps on the right of the ridge on the roof are used in the profile. The mean C_p profiles along these lines are shown in Fig. 17. In Fig. 17, d represents the distance along the building surface and h is the eave height of the building. Between ABL and IJ, the mean C_p profiles follow similar trends for all three building orientations with almost same values on the windward wall for all three cases. The largest variation of mean C_p is found on the roof close to the leading edge. The mean suction on the roof close to the leading edge is higher in ABL flow compared to that in the IJ flow.

Mean C_p profiles along the mid-line of the low-rise building studied here are also compared with that of a cubic building studied by Chay and Letchford (2002) (Fig. 18). The C_p values presented in Fig. 18 from Chay and Letchford (2002) are also based on atmospheric pressure as the reference static pressure and the maximum velocity as the reference velocity. Notable difference is observed for the mean C_p distribution on the windward face, where the distribution is uniform in Chay and Letchford (2002) but not in the present study. This is due to more uniform velocity distribution across the building height in Chay and Letchford (2002) compared to that in the present study (Fig. 9). Castro and Robins (1977) observed similar behaviour of mean C_p distributions on the windward face of a cube while comparing between uniform and boundary layer incoming flows.

4.1.2 Pressure coefficients – standard deviation

Pressure fluctuations on the building surfaces are shown in Fig. 19 in terms of standard deviation of C_p for both IJ and ABL flows. In general, the higher pressure fluctuations on the roof and on the side walls close to the leading edge are associated with unsteady flow phenomena such as flow separation and reattachment. The largest fluctuations are observed for the corner angle case at the leading edge corner on the roof for both ABL and IJ flows (Figs. 19(c), (f)). Fig. 20 shows that C_p fluctuations are generally higher in ABL compared to those in IJ, which could be attributed to the overall higher turbulence intensity in the ABL than IJ; and that the distribution of the fluctuation is less uniform and symmetric about the direction of the wind flow for 0° and 90° wind directions (see Fig. 4 for wind direction convention) in IJ compared to that in ABL.

Profiles of C_p standard deviation along the line of pressure taps in Fig. 16 are shown in Fig. 20. Pressure fluctuations are higher on the windward wall and on the roof close to the leading edge ($0 < d/h < 2$) for ABL compared to those in IJ. Although the standard deviation is higher in the leading edge corner zone on the roof for ABL than for IJ, along the line of pressure taps at which the profiles are plotted, the IJ produced higher fluctuation in one particular tap at $d/h=1.13$ than ABL. The differences in the nature of the flows, straight line winds in ABL and radially diverging flow in IJ, could have attributed to this difference in pressure fluctuations.

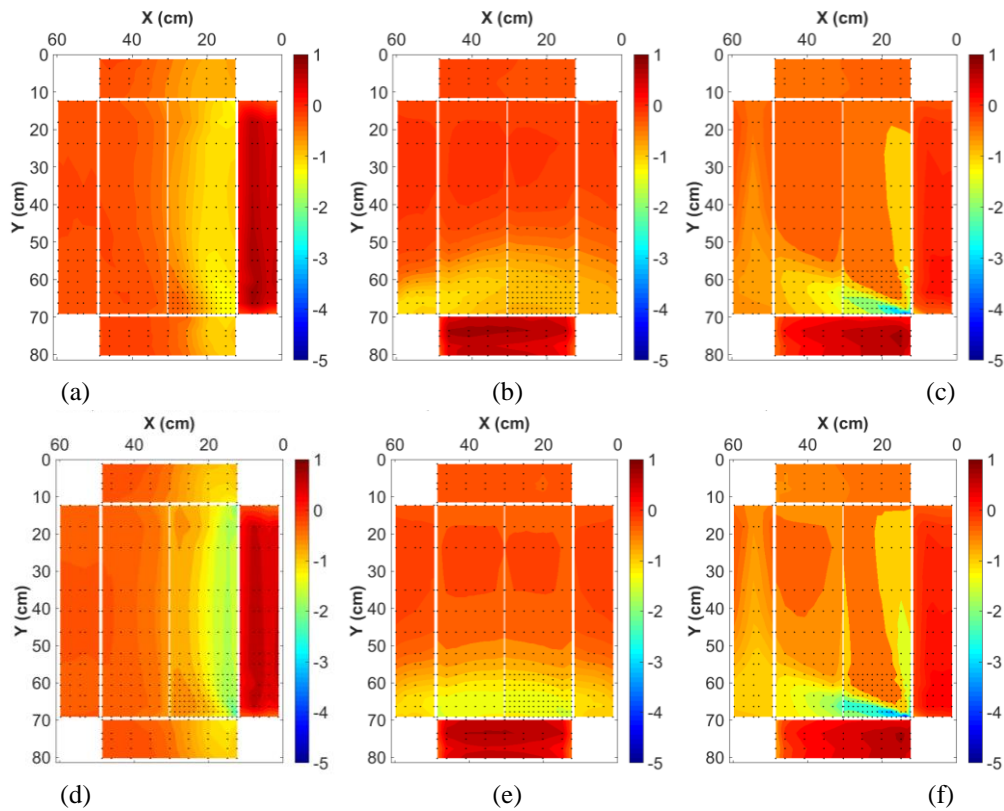


Fig. 15 Mean C_p contours for (a) IJ Case 1, (b) IJ Case 2, (c) IJ Case 3, (d) ABL 0° , (e) ABL 90° and (f) ABL 57°

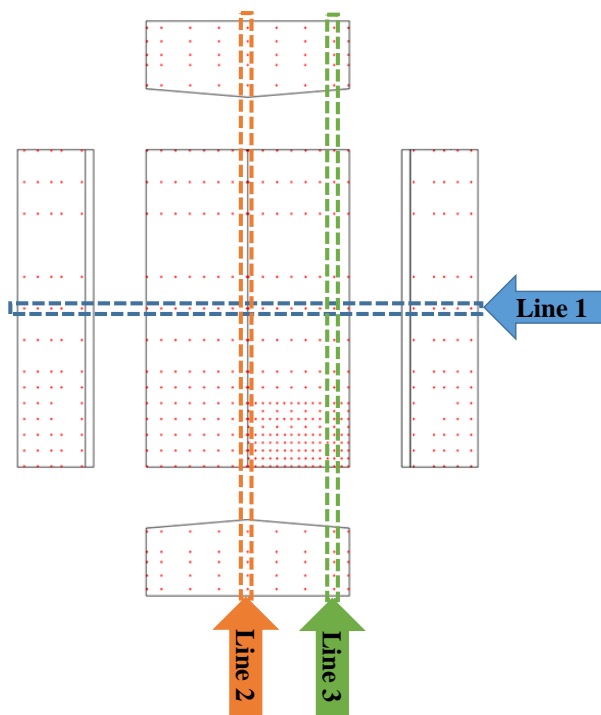


Fig. 16 Line of taps along which the C_p profiles are plotted

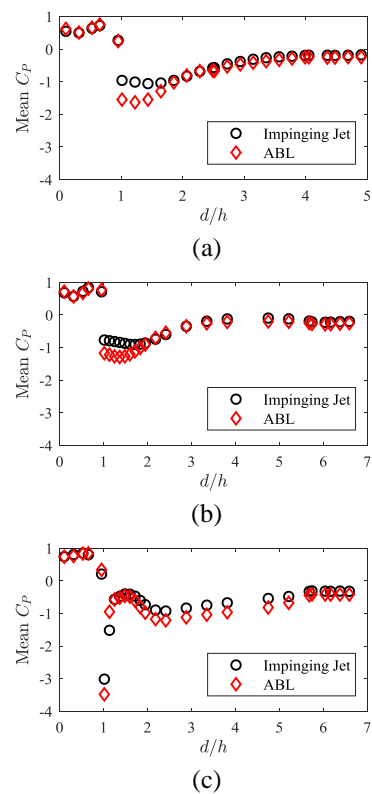


Fig. 17 Comparison of the mean C_p profiles between IJ and ABL flows for (a) Case 1 - 0° (Line 1), (b) Case 2 - 90° (Line 2) and (c) Case 3 - 57° (Line 3)

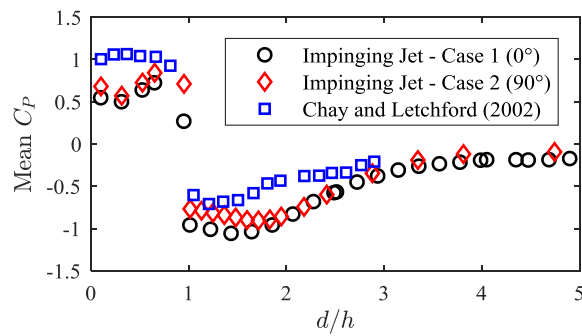


Fig. 18 Comparison of the mean C_p profiles between the present study and the study by Chay and Letchford (2002)

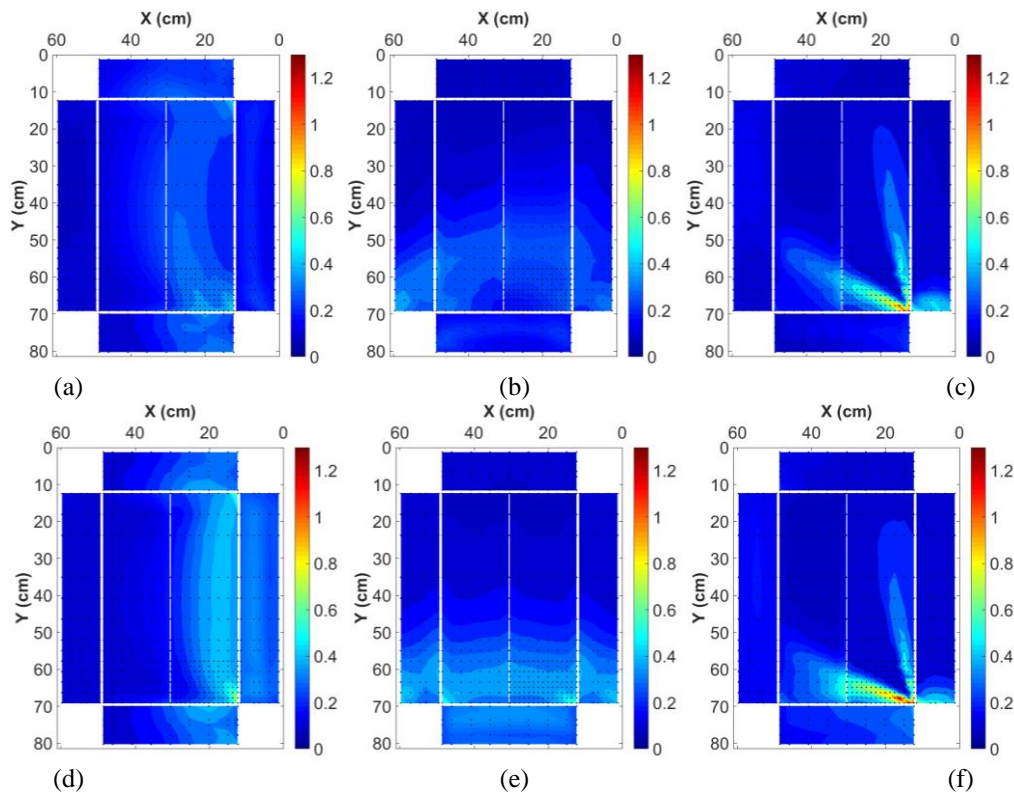


Fig. 19 Standard deviation of C_p contours for (a) IJ Case 1, (b) IJ Case 2, (c) IJ Case 3, (d) ABL 0° , (e) ABL 90° and (f) ABL 57°

4.1.3 Peak pressure coefficients

3 s peak pressure coefficients are basis for design wind loads for many building codes around the world (e.g., ASCE 7-10 2013). Therefore, the 3 s peak pressure coefficients are also calculated on the surfaces of the building for both the IJ and ABL flows and using extreme value estimator proposed by Lieblein (Lieblein 1974), also known as Lieblein BLUE (Best Linear Unbiased Estimator). Note that the dynamic pressure in the 3 s peak pressure coefficient calculation is based on 3 s peak wind velocity. Also note that here the duration 3 s is in full scale. Contours of the 3 s peak C_p s are shown in Fig. 21 whereas the profiles are shown in Fig. 22. Overall distribution of the 3 s peak C_p s on the building surfaces between ABL and IJ flows are very much similar. However, upon closer

inspection, higher suction is observed at the leading edge corner on the roof for the IJ flow compared to that in the ABL flow, especially for the corner angle case (Figs. 21(c), (f)). Similar conclusion can be drawn from the profile plot shown in Fig. 22(c). About 20.1% difference is observed between the minimum 3 s peak C_p s out of all pressure taps from ABL and IJ for the corner angle case, with IJ producing higher suction. Corner wind angle cases are usually the most critical as they can produce the maximum suction on the roof during a wind event. From that perspective, for the present study, intermediate wind event simulated by IJ would produce slightly higher local loading compared to that in straight winds like ABL flow based on local 3 s peak pressures comparison.

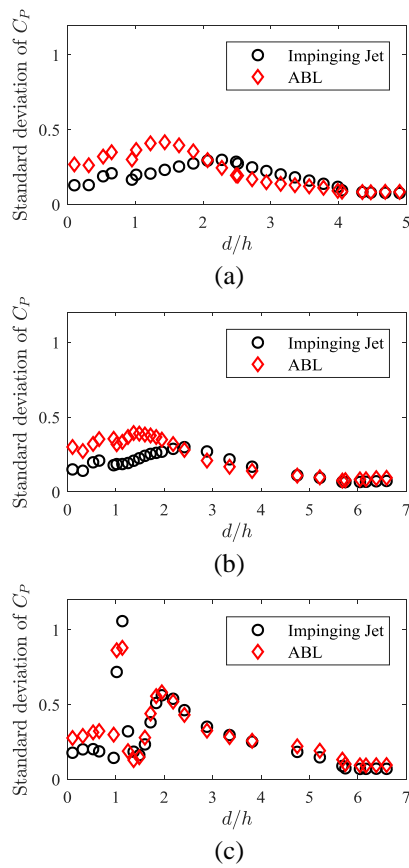


Fig. 20 Comparison of the standard deviation of C_p profiles between IJ and ABL flows for (a) Case 1 - 0° (Line 1), (b) Case 2 - 90° (Line 2) and (c) Case 3 - 57° (Line 3)

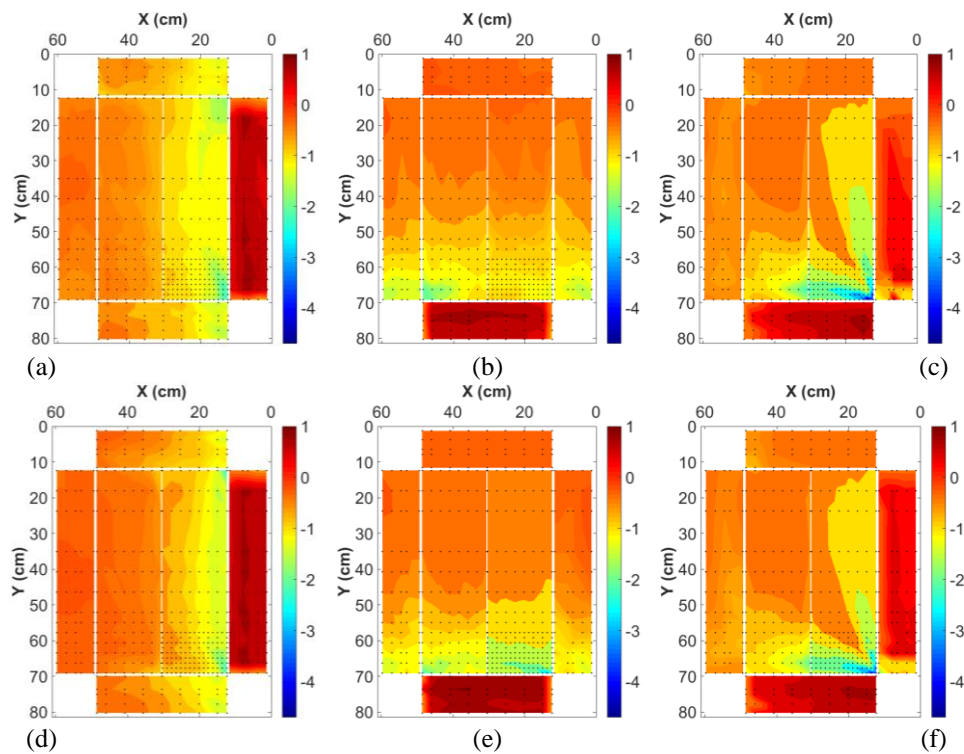


Fig. 21 3 s peak C_p contours for (a) IJ Case 1, (b) IJ Case 2, (c) IJ Case 3, (d) ABL 0° , (e) ABL 90° and (f) ABL 57°

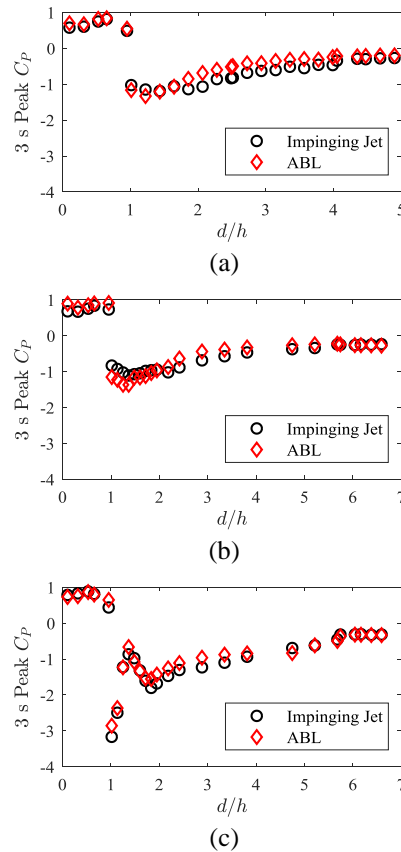


Fig. 22 Comparison of 3 s peak of C_p profiles between IJ and ABL flows for (a) Case 1 - 0° (Line 1), (b) Case 2 - 90° (Line 2) and (c) Case 3 - 57° (Line 3)

Table 2 Comparison of design pressures between WindEEE Dome, NIST Database and ASCE 7-10

Zones	A	B	C	D	E	F	G	H
WindEEE Dome IJ (psf)	55	-3	42	-2	-63	-56	-41	-23
WindEEE Dome ABL (psf)	65	-3	52	-3	-81	-72	-56	-32
NIST Database (psf)	72	-3	48	-3	-59	-70	-44	-22
ASCE 7-10 (psf)	77	-40	51	-24	-92	-52	-64	-41

4.2 Comparison with ASCE 7-10

The 3 s peak surface pressures for the IJ are also compared with the design wind pressures (in terms of pounds per square foot, psf) provided in the ASCE 7-10 code (ASCE 7-10 2013). ASCE 7-10 provides design pressures for synoptic wind events in the atmosphere for different sizes and shapes of buildings. Method 2 of the Envelope Procedure from ASCE 7-10 is adopted for this comparison. In order to apply a design wind speed for this comparison, the design wind speed for Miami, Florida is chosen. According to ASCE 7-10, the design wind speed near Miami, Florida is 180 mph (80.5 m s^{-1}) at 10 m. The climate of Miami is mixed with various tropical systems that produce strong thunderstorms with frequent lightning and heavy rain. The design wind speed is based on statistical data at specific geographical locations. This data

do not discern between synoptic and non-synoptic events. Therefore, the wind loads on the building for IJ, ABL flow at WindEEE Dome and NIST Database are calculated for the same design wind speed (80.5 m s^{-1}) to investigate the difference in wind loads on the same building for different flow types.

In the ASCE 7-10 code, the design pressures are reported in terms of different zones on the surfaces of the building. Area weighted average of pressure was calculated based on the point pressure measurements from the experiment for the zones defined in ASCE 7-10. Comparisons of design pressures between ASCE 7-10 and the IJ flow are provided in Table 2. Wind pressures from three ABL cases (0° , 57° and 90° wind directions) from WindEEE Dome as well as from the NIST Aerodynamic Database (UWO Data Sets) (Ho *et al.* 2005) are also included in Table 2. For all three different cases presented

in Table 2 (WindEEE Dome IJ, WindEEE Dome ABL and NIST Database), wind loads are lower or very close to the ASCE recommended design wind loads at every zones except Zone F. Zone F, which is on the roof (ASCE 7-10), experiences higher wind loads than ASCE 7-10 not only for IJ but also for ABL flows at WindEEE Dome and NIST Database. Further investigations are needed to explain the reasoning behind the ASCE code not being conservative in Zone F even for ABL flow cases.

5. Conclusions

In an effort to better understand the effect of stationary non-Gaussian winds on the wind loads of a typical low-rise building, a series of tests has been performed in the large test chamber at the WindEEE Dome. A continuous radial impinging jet (IJ) was used for the first time to replicate an intermediate (i.e., stationary but non-Gaussian) wind event recorded at the Port of La Spezia in Italy. The experiment was designed to quantitatively investigate the effects of these intermediate wind events on the building surface pressure distributions for three different building orientations. In addition, pressure distributions on the same building model for atmospheric boundary layer (ABL) flow (i.e., stationary and Gaussian) at the WindEEE Dome are compared with the pressure distributions from the IJ flow. Moreover, wind loads at different zones, as defined by the ASCE building code (ASCE 7-10 2013), are calculated and compared among WindEEE Dome IJ, WindEEE Dome ABL, NIST Aerodynamic Database and the code itself.

The intermediate wind event created by the continuous radial IJ at WindEEE is stationary with statistical non-Gaussian properties similar to the event recorded at the Port of La Spezia in Italy. Skewness, kurtosis, peak wind speed, gust factor and turbulence intensity between the two records (WindEEE and full scale) are compared to characterize the IJ flow at WindEEE Dome as well as to obtain scales. Corresponding scales between WindEEE Dome and full scale event are; velocity 1:1.2, time 1:84 and length 1:101.

The mean pressure coefficient (C_p) distributions on the building surfaces are found to be similar between the IJ and the ABL cases, with mean roof suction higher on the roof close to the eave for ABL compared to that in IJ (difference in minimum mean C_{ps} is 16.5%). However, when 3 s peak C_{ps} are compared, the IJ produced localized higher roof suction than ABL especially for the corner angle case (difference in minimum 3 s peak C_p s is 20.1%). Fluctuations of C_{ps} , represented by standard deviation, are higher in ABL compared to those in the IJ (difference in maximum standard deviation of C_{ps} is 14.3%). Noticeable difference in C_p fluctuations between IJ and ABL is observed in the distribution of standard deviation of C_p on the building surface where distribution is less symmetric and uniform for IJ than ABL. Apart from the non-Gaussian characteristics of IJ, the differences in velocity profiles and building height turbulence intensities between ABL and IJ could have influenced C_{ps} . When wind loads are compared with the ASCE standard, it is found that except for one zone on the roof (Zone F), the ASCE standard provides

conservative design loads for the building orientations (0° , 57° and 90°) tested in this study.

At the end, it is important to acknowledge that this topic deserves a lot of additional research from experimental point of view. This paper presented an attempt to experimentally simulate this class of winds using IJ approach, but other options will also be explored in the future. While this study is a continuation of the work by Kasperski (2002) and De Gaetano *et al.* (2014), it can also serve as the starting point for experimental research of non-Gaussian, stationary wind events. At the same time, it is equally important to have more complete understanding of these winds regarding their dynamics and climatology at full scale. This gap of knowledge regarding experimental investigation of intermediate winds, on one side, and their meteorological description, on the other side, calls for an interdisciplinary research initiative between wind engineering and atmospheric sciences communities (Solari 2014). Such an interdisciplinary as well as multiscale study had recently been performed for a downburst event in the Mediterranean (Burlando *et al.* 2017). In addition, the experiments in this study were compared against a single full-scale event. Lastly, in order to draw general conclusions regarding wind actions from intermediate winds an ensemble averaging of multiple non-Gaussian wind events is needed.

Acknowledgments

This work was made possible through the Canada Foundation for Innovation “The Wind Engineering Energy and Environment (WindEEE) Dome” Infrastructure Operational Fund (Grant number: X2281838). The authors would like to thank Professor Giovanni Solari and Dr. Patrizia De Gaetano for providing us raw data and metadata for the intermediate event reported in De Gaetano *et al.*, (2014). The authors would also like to acknowledge Dr. Ahmed Elatar for his help during the testing performed at the WindEEE Dome as well as the post processing of some of the experimental data.

References

- AS / NZS 1170.2:2011. (2015), “Structural design actions - Part 2: Wind actions” (Sep. 14, 2015).
- ASCE 7-10. (2013), *Minimum Design Loads for Buildings and Other Structures*. Standards, American Society of Civil Engineers.
- Burlando, M., Romanić, D., Solari, G., Hangan, H. and Zhang, S. (2017), “Field data analysis and weather scenario of a downburst event in Livorno, Italy, on 1 October 2012”, *Mon. Weather Rev.*, **145**(9), 3507-3527. <https://doi.org/10.1175/MWR-D-17-0018.1>.
- Castro, I.P. and Robins, A.G. (1977), “The flow around a surface-mounted cube in uniform and turbulent streams”, *J. Fluid Mech.*, **79**(2), 307-335. <https://doi.org/10.1017/S0022112077000172>.
- Cermak, J.E. (1971), “Laboratory simulation of the atmospheric boundary layer”, *AIAA J.*, **9**(9), 1746-1754. <https://doi.org/10.2514/3.49977>.
- Chay, M.T., Albermani, F. and Wilson, R. (2006), “Numerical and

- analytical simulation of downburst wind loads”, *Eng. Struct.*, **28**(2), 240-254. <https://doi.org/10.1016/j.engstruct.2005.07.007>.
- Chay, M.T. and Letchford, C.W. (2002), “Pressure distributions on a cube in a simulated thunderstorm downburst—Part A: stationary downburst observations”, *J. Wind Eng. Ind. Aerod.*, **90**(7), 711-732. [https://doi.org/10.1016/S0167-6105\(02\)00158-7](https://doi.org/10.1016/S0167-6105(02)00158-7).
- Chen, L. and Letchford, C.W. (2004a), “A deterministic–stochastic hybrid model of downbursts and its impact on a cantilevered structure”, *Eng. Struct.*, **26**(5), 619-629. <https://doi.org/10.1016/j.engstruct.2003.12.009>.
- Chen, L. and Letchford, C.W. (2004b), “Parametric study on the along-wind response of the CAARC building to downbursts in the time domain”, *J. Wind Eng. Ind. Aerod.*, **92**(9), 703-724. <https://doi.org/10.1016/j.jweia.2004.03.001>.
- Choi, E.C. and Hidayat, F.A. (2002), “Dynamic response of structures to thunderstorm winds”, *Progress Struct. Eng. Mater.*, **4**(4), 408-416. <https://doi.org/10.1002/pse.132>.
- Cook, N.J., Ian Harris, R. and Whiting, R. (2003), “Extreme wind speeds in mixed climates revisited”, *J. Wind Eng. Ind. Aerod.*, **91**(3), 403-422. [https://doi.org/10.1016/S0167-6105\(02\)00397-5](https://doi.org/10.1016/S0167-6105(02)00397-5).
- De Gaetano, P., Repetto, M.P., Repetto, T. and Solari, G. (2014), “Separation and classification of extreme wind events from anemometric records”, *J. Wind Eng. Ind. Aerod.*, **126**, 132-143. <https://doi.org/10.1016/j.jweia.2014.01.006>.
- ESDU. (1982), *Strong winds in the atmospheric boundary layer. Part 1: Mean hourly wind speeds*.
- ESDU. (1983), *Strong winds in the atmospheric boundary layer. Part 2: Discreet gust speeds*.
- ESDU. (1985), *Characteristics of atmospheric turbulence near the ground*.
- Haan, F.L., Balaramudu, V.K. and Sarkar, P.P. (2010), “Tornado-Induced Wind Loads on a Low-Rise Building”, *J. Struct. Eng.*, **136**(1), 106-116. [https://doi.org/10.1061/\(ASCE\)ST.1943-541X.0000093](https://doi.org/10.1061/(ASCE)ST.1943-541X.0000093).
- Gomes, L. and Vickery, B.J. (1977), “Extreme wind speeds in mixed climates”, *J. Wind Eng. Ind. Aerod.*, **2**, 331-344. [https://doi.org/10.1016/0167-6105\(78\)90018-1](https://doi.org/10.1016/0167-6105(78)90018-1).
- Hangan, H. (2010), “Current and future directions for wind research at Western: A new quantum leap in wind research through the Wind Engineering, Energy and Environment (WindEEE) Dome”, *Wind Engineers, JAWE*, **35**(4), 277-281. <https://doi.org/10.5359/jawe.35.277>.
- Hangan, H. (2014), “The Wind Engineering Energy and Environment (WindEEE) Dome at Western University, Canada”, *Wind Engineers, JAWE*, **39**(4), 350-351. <https://doi.org/10.5359/jawe.39.350>.
- Hangan, H., Refan, M., Jubayer, C., Parvu, D. and Kilpatrick, R. (2017a), “Big data from big experiments. The WindEEE dome”, *Whither Turbulence and Big Data in the 21st Century?*, A. (Eds., Pollard, L. Castillo, L. Danaila, and M. Glauser), Springer International Publishing.
- Hangan, H., Refan, M., Jubayer, C., Romanic, D., Parvu, D., LoTufo, J. and Costache, A. (2017b), “Novel techniques in wind engineering”, *J. Wind Eng. Ind. Aerod.*, **171**, 12-33. <https://doi.org/10.1016/j.jweia.2017.09.010>.
- Hangan, H., Romanic, D. and Jubayer, C. (2019), “Three-dimensional, non-stationary and non-Gaussian (3D-NS-NG) wind fields and their implications to wind–structure interaction problems”, *J. Fluid. Struct.*, In press.
- Ho, T.C.E., Surry, D., Morrish, D. and Kopp, G.A. (2005), “The UWO contribution to the NIST aerodynamic database for wind loads on low buildings: Part 1. Archiving format and basic aerodynamic data”, *J. Wind Eng. Ind. Aerod.*, **93**(1), 1-30. <https://doi.org/10.1016/j.jweia.2004.07.006>.
- Holmes, J.D. (2015), *Wind Loading of Structures, 3rd Edition*. CRC Press.
- Holmes, J.D., Hangan, H.M., Schroeder, J.L., Letchford, C.W., and Orwig, K.D. (2008), “A forensic study of the Lubbock-Reese downdraft of 2002”, *Wind Struct.*, **11**(2), 137-152. <https://doi.org/10.12989/was.2008.11.2.137>.
- Holmes, J.D. and Oliver, S.E. (2000), “An empirical model of a downburst”, *Eng. Struct.*, **22**(9), 1167-1172. [https://doi.org/10.1016/S0141-0296\(99\)00058-9](https://doi.org/10.1016/S0141-0296(99)00058-9).
- Irwin, H.P.A.H., Cooper, K.R. and Girard, R. (1979), “Correction of distortion effects caused by tubing systems in measurements of fluctuating pressures”, *J. Wind Eng. Ind. Aerod.*, **5**(1), 93-107. [https://doi.org/10.1016/0167-6105\(79\)90026-6](https://doi.org/10.1016/0167-6105(79)90026-6).
- Jubayer, C., Elatar, A. and Hangan, H. (2016), “Pressure distributions on a low-rise building in a laboratory simulated downburst, 8th International Colloquium on Bluff Body Aerodynamics and Applications”, Boston, Massachusetts, USA.
- Jubayer, C.M. and Hangan, H. (2016), “A numerical approach to the investigation of wind loading on an array of ground mounted solar photovoltaic (PV) panels”, *J. Wind Eng. Ind. Aerod.*, **153**, 60-70. <https://doi.org/10.1016/j.jweia.2016.03.009>.
- Junayed, C., Jubayer, C., Parvu, D., Romanic, D. and Hangan, H. (2019), “Flow field dynamics of large-scale experimentally produced downburst flows”, *J. Wind Eng. Ind. Aerod.*, **188**, 61-79. <https://doi.org/10.1016/j.jweia.2019.02.008>.
- Kasperski, M. (2002), “A new wind zone map of Germany”, *Journal of Wind Engineering and Industrial Aerodynamics, 3rd European-African Conference on Wind Engineering (Part two)*, **90**(11), 1271-1287.
- Kim, J., Hangan, H. and Eric Ho, T.C. (2007), “Downburst versus boundary layer induced wind loads for tall buildings”, *Wind Struct.*, **10**(5), 481-494. <https://doi.org/10.12989/was.2007.10.5.481>.
- Kwon, D.K. and Kareem, A. (2013), “Generalized gust-front factor: A computational framework for wind load effects”, *Eng. Struct.*, **48**, 635-644. <https://doi.org/10.1016/j.engstruct.2012.12.024>.
- Kwon, D. and Kareem, A. (2009), “Gust-front factor: New framework for wind load effects on structures”, *J. Struct. Eng.*, **135**(6), 717-732. [https://doi.org/10.1061/\(ASCE\)0733-9445\(2009\)135:6\(717\)](https://doi.org/10.1061/(ASCE)0733-9445(2009)135:6(717)).
- Letchford, C.W. and Chay, M.T. (2002), “Pressure distributions on a cube in a simulated thunderstorm downburst. Part B: moving downburst observations”, *J. Wind Eng. Ind. Aerod.*, **90**(7), 733-753. [https://doi.org/10.1016/S0167-6105\(02\)00163-0](https://doi.org/10.1016/S0167-6105(02)00163-0).
- Letchford, C.W., Mans, C. and Chay, M.T. (2002), “Thunderstorms—their importance in wind engineering (a case for the next generation wind tunnel)”, *Journal of Wind Engineering and Industrial Aerodynamics, Fifth Asia-Pacific Conference on Wind Engineering*, **90**(12-15), 1415-1433.
- Lieblein, J. (1974), *Efficient methods of extreme-value methodology*. Institute for Applied Technology, National Bureau of Standards, Washington, DC, USA.
- Lombardo, F.T., Main, J.A. and Simiu, E. (2009), “Automated extraction and classification of thunderstorm and non-thunderstorm wind data for extreme-value analysis”, *J. Wind Eng. Ind. Aerod.*, **97**(3), 120-131. <https://doi.org/10.1016/j.jweia.2009.03.001>.
- McConville, A.C., Sterling, M. and Baker, C.J. (2009), “The physical simulation of thunderstorm downbursts using an impinging jet”, *Wind Struct.*, **12**(2), 133-149. <http://dx.doi.org/10.12989/was.2009.12.2.133>.
- Mishra, A.R., James, D.L. and Letchford, C.W. (2008), “Physical simulation of a single-celled tornado-like vortex, Part B: Wind loading on a cubical model”, *J. Wind Eng. Ind. Aerod.*, **96**(8), 1258-1273. <https://doi.org/10.1016/j.jweia.2008.02.027>.
- NBCC 2010. (2012), “National Building Code of Canada 2010 - National Research Council Canada”, abstract, <http://www.nrc-cnrc.gc.ca/eng/publications/codes_centre/2010_national_buidin_g_code.html> (Sep. 14, 2015).

- Refan, M., Hangan, H. and Wurman, J. (2014), "Reproducing tornadoes in laboratory using proper scaling", *J. Wind Eng. Ind. Aerod.*, **135**, 136-148. <https://doi.org/10.1016/j.jweia.2014.10.008>.
- Repetto, M.P., Burlando, M., Solari, G., De Gaetano, P. and Pizzo, M. (2017), "Integrated tools for improving the resilience of seaports under extreme wind events", *Sustainable Cities and Society*, **32**, 277-294. <https://doi.org/10.1016/j.scs.2017.03.022>.
- Sengupta, A. (2007), "Study of microburst-induced wind flow and its effects on cube-shaped buildings using numerical and experimental simulations of an impinging jet", Iowa State University, Ames, Iowa, USA.
- Sengupta, A. and Sarkar, P.P. (2008), "Experimental measurement and numerical simulation of an impinging jet with application to thunderstorm microburst winds", *J. Wind Eng. Ind. Aerod.*, **96**(3), 345-365. <https://doi.org/10.1016/j.jweia.2007.09.001>.
- Solari, G. (2014), "Emerging issues and new frameworks for wind loading on structures in mixed climates", *Wind Struct.*, **19**(3), 295-320. <https://doi.org/10.12989/was.2014.19.3.295>.
- Solari, G., Burlando, M., De Gaetano, P. and Repetto, M.P. (2015), "Characteristics of thunderstorms relevant to the wind loading of structures", *Wind Struct.*, **20**(6), 763-791. <https://doi.org/10.12989/was.2015.20.6.763>.
- Solari, G., Repetto, M.P., Burlando, M., De Gaetano, P., Pizzo, M., Tizzi, M. and Parodi, M. (2012), "The wind forecast for safety management of port areas", *Journal of Wind Engineering and Industrial Aerodynamics, 13th International Conference on Wind Engineering*, **104**, 266-277.
- Surry, D. and Stathopoulos, T. (1978), "An experimental approach to the economical measurement of spatially-averaged wind loads", *J. Wind Eng. Ind. Aerod.*, **2**(4), 385-397. [https://doi.org/10.1016/0167-6105\(78\)90021-1](https://doi.org/10.1016/0167-6105(78)90021-1).
- Uematsu, Y. and Isyumov, N. (1999), "Wind pressures acting on low-rise buildings", *J. Wind Eng. Ind. Aerod.*, **82**(1), 1-25. [https://doi.org/10.1016/S0167-6105\(99\)00036-7](https://doi.org/10.1016/S0167-6105(99)00036-7).
- Xu, Z. and Hangan, H. (2008), "Scale, boundary and inlet condition effects on impinging jets", *J. Wind Eng. Ind. Aerod.*, **96**(12), 2383-2402. <https://doi.org/10.1016/j.jweia.2008.04.002>.
- Zhang, Y., Sarkar, P. and Hu, H. (2013), "An experimental study of flow fields and wind loads on gable-roof building models in microburst-like wind", *Exp. Fluid.*, **54**(5), 1-21.